Title

Human semicircular canal form: Ontogenetic changes and variation of shape and size.

Short running title: Ontogenic changes of the human semicircular canal form

Authors names:

Cárdenas-Serna, Marcela

Jeffery, Nathan

Affiliations

Department of Musculoskeletal Biology, Institute of Life Course and Medical Sciences, University of Liverpool

Abstract

The semicircular canals transduce angular acceleration of the head into neuronal signals and their morphology has been used to infer function. Once formed, the bony labyrinth, that surrounds the canals, is tightly regulated and has a very low bone turnover. However, relaxed postnatal inhibition of bone remodelling later in ontogeny may allow for some organised adjustments of shape and size or for greater stochastic variation. In the present study, we test the hypotheses that after birth the shape and size of the bony canal changes or becomes more variable, or both. We study microCT scans of human perinatal and adult temporal bones using a combination of geometric morphometric analysis and cross-sectional measures. Results revealed marginal differences of size (<5%), of cross-sectional shape and of measurement variability. Geometry of the three canals together and their cross-sectional areas were, however, indistinguishable between perinates and adults. These mixed findings are indicative of diminutive levels of relaxed inhibition superimposed over a constrained template of semicircular canal morphology.

Keywords

Semicircular canals, bony labyrinth, microCT, inner ear, geometric morphometrics.

Introduction

The vestibular apparatus is responsible for detecting linear and angular accelerations of the head and consists of the saccule, utricle, and three roughly-orthogonal semicircular canals embedded within the petrous temporal bone. These canals transduce angular acceleration of the head into proprioceptive neuronal signals coded for time and motion in three dimensions (Berlin et al. , 2013) and contain two main parts: an outer bony canal, filled with perilymph and an inner membranous canal filled with endolymph. Signal mechanotransduction occurs in the ampulla, inside the membranous labyrinth. There, the cilia of hair cells — embedded within the cupula — are mechanically deformed by inertial flow of the endolymph.

Notwithstanding cupula mechanics, the sensitivity of the canals to angular acceleration depends largely on the volume of fluid displaced by inertia, which in turn depends on canal length and cross-sectional area (see Jones and Spells, 1963; Lambert et al., 2008; Yang and Hullar, 2007, 2007; Iversen and Rabbitt, 2017). However, by maximising volume displacement the limits of cilia deflection are reached sooner, which in turn limits the frequency range over which the canal can operate effectively. Slender rather than shorter canals are invariably favoured as an evolutionary compromise, possibly because narrowing has the added advantages of diminishing viscous blocking as well as promoting Poiseuille flow (Obrist, 2019). These qualities are manifested in the empirically

well-established relationship between canal length, approximated by the radius of curvature of the canals, and postural behaviour. Back as early as 1908, Gray noted that the size of the semicircular canals appeared to correlate with the flying abilities of different species (Gray, 1908). Since then, numerous studies have used the radius of curvature, or variations thereof, to infer the locomotor repertoire and agility of extant and extinct taxa (Rabbitt et al., 2004; Spoor et al., 2007; Walker et al., 2008; David et al., 2010; Ryan et al., 2012; Le Maitre et al., 2017) subject to appropriate adjustments for body size scaling effects (Spoor and Zonneveld, 1998; Spoor et al., 2007).

Canal sensitivity is also influenced by the vector as well as the volume of endolymphatic flow, requiring encoding afferent signals from all six canals (Rabbitt, 1999). Hence, the planar relationships of the canals to each other as well as to the principal axes of eye and head motion influence how well the direction of angular acceleration is detected (Van Buskirk, 1988; Rabbitt, 1999; Cox and Jeffery, 2010). In humans, ipsilateral canals are mostly orthogonal to each other (Blanks et al., 1985) although they do not lie at exact right angles (Lee et al., 2013). Pairs of contralateral canals are mostly parallel to each other, but with deviations up to 12° (Blanks et al., 1985). Additionally, the semicircular canals do not lie in a single plane, but rather exhibit out-of-plane deviations, or torsion, that are thought to increase the sensitivity of the canal by broadening the range of planes of angular acceleration that can stimulate endolymphatic flow (Tremble, 1929; Muren et al., 1986). Notably, however, the anatomical plane of the canal and the plane of maximal response are not the same, differing on average by 10° (Rabbitt, 1999). Features such as ellipticity (or deviation from circularity) of the circuit are also considered important attributes, particularly in accommodating relatively longer, and therefore more sensitive, canals in smaller crania (Goyens, 2019).

Because canal form is so tightly correlated with sensitivity as well as operational range, the conservation of form throughout life is presumed to be critical to maintain reflexes and functions, namely locomotion, and to avoid potentially deleterious phenotypic variants. Indeed, inner ear development is remarkably precocious. Unlike any other organ system, the general adult spatial arrangement and size of the canals are mostly achieved in utero for a range of different mammals (Jeffery and Spoor, 2004; Ishikawa et al., 2018; see also: Hoyte, 1961; Ekdale, 2010). Furthermore, subsequent adaptation of the perilabyrinthine bone is also inhibited (Frisch et al., 2000), presumably to prevent bone remodelling stimulated by mechanical forces that propagate through the petrous bone (e. g. masticatory forces). The notional mechanism behind this inhibition is increased levels of osteoprotegerin (OPG) within the perilymph (Zehnder et al., 2005), which then enters the surrounding bone through the lacuno-canalicular system. The persistence and permeability of these canaliculi are entirely dependent on the presence of viable osteocytes to maintain the system. In early life, more viable osteocytes are located centripetally in the perilabyrinthine bone. Around 20%

of viable osteocytes are lost during the first three years of life, with a much smaller decline of osteocytes in later years (Bloch et al., 2012). The remaining osteocytes slowly shift the distribution centrifugally (Bloch and Sørensen, 2010), which may impede the diffusion of OPG radially. This may cause a disinhibition of bone remodelling, or may be superfluous to maintaining sufficient inhibition. Here we test the hypothesis that remodelling is indeed disinhibited postnatally by scrutinising morphological outcomes for evidence of 1) organised postnatal change, possibly allowing for functional refinements; 2) disorganised, stochastic, variation as part of a general entropic trend with age. Organised change predicts that perinatal canals are subtly different from adults in ways not previously captured by conventional metrics (e.g. Jeffery and Spoor, 2004) whereas disorganised change would be evidenced by canals that may be similar on average but less variable than those seen amongst adults. Here we test both predictions using microCT data representing adult and perinatal modern humans together with methods that can capture and analyse more detail than in previous studies.

Methods

General considerations and sample collection

For this study, we employed two sets of analyses. First, a geometric morphometric analysis of shape with landmarks placed across all three canals. The totality of the shape represented by said landmarks will be referred to as configuration shape. Second, a cross-sectional morphometric analysis along the centrelines of each canal. For both analyses, endocasts of human semicircular canals (SCC) obtained from micro computed tomography (µCT) were used.

Samples were collected as follows. The young cohort was comprised of 51 perinatal unarticulated petrous temporal bones. They were obtained from the University of Liverpool's MeCoMa collection, which consists of perinatal bone specimens collected from the Brownlow Hill workhouse in Liverpool, England, during the 19th century. Out of the 51 specimens, two were discarded due to fractures on the superior semicircular canal and one was left out due to having an abnormally small lateral canal. The adult cohort was comprised of 48 specimens, of which 17 were obtained from the bone collection at the Human Anatomy Resource Centre, the University of Liverpool (unknown gender and age). All specimens collected from the University of Liverpool were collected and analysed with approval of the Health and Life Sciences Research Ethics Committee (reference number 5504). An additional group of 16 adult specimens was collected from cadavers donated to the Anatomy department, the University of Cambridge. The latter dataset had an average age of 84.8 years (SD: 9.3, Median: 86). The remaining 15 specimens were obtained from an online repository (Wimmer et al., 2019). Specimens collected at the University of Liverpool were µCT

scanned using a SkyScan 1272 Micro-X-ray CT (Bruker) with an isotropic resolution of 13 microns (perinates: 60Kv; 166uA;0.25mm Al filter. adults: 100Kv; 100uA;0.11mm Cu filter). The dataset from University of Cambridge were scanned at approximately 24 microns (125 kV; 120 µA; no filter). The specimens from the online repository were scanned at approximately 60 microns. Because of the nature of our samples, biometric data were limited. Although the specimens used were all accurately classified as perinates or adults, no data pertaining to sex nor exact chronological age or ethnicity were available, except for the age of the subset of adult samples from Cambridge. A summary of each dataset and the analyses they were included in can be seen in Table 1. Available biometric and image resolution details for each specimen are provided in the supplementary materials.

Segmentation of endocasts

The acquired images were imported into ImageJ (1.53a v NIH, USA). For each stack, a plot profile was created and the threshold value was calculated by the half maximum height (HMH) technique (Spoor and Zonneveld, 1995) with reference to the bone and canal lumen values. Ten measurements were taken for each specimen at different locations throughout the stack. The stacks were then imported into Amira (Version 6.0.0, Thermo Fisher Scientific). Segmentation of the canals was carried out by thresholding, using the mean HMH values previously calculated. The segmented area representing the lumen of the canals and the vestibule was then saved as a labelmap. A surface generated from the labelmap can be seen in Figure 1, A.

For subsequent analyses, the centrelines of each canal were computed. To find the centrelines, the labelmaps were down-sampled and the Distance-ordered thinner (Len of ends: 10) and the Trace line modules were used, which generated a line set. This resulting line set was edited using the Filament Editor, to remove unwanted branching lines (Figure 1, B). The Smooth lineset module was then used (smooth: 0.9; attach to data: 0.05; Number of iterations: 100). Lastly, the line set was trimmed at the point where the canals meet the vestibule (Figure 1, C). The centrelines were divided, so that one line segment was generated for each canal, and one for the common crus.

Geometric morphometric analysis

Shape configuration was analysed using a landmark-based geometric morphometric (GMM) approach (Bookstein, 1991, 1996). This method is a quantitative way of analysing shape. In GMM, shape is defined as the geometric information remaining after removing scale, location and orientation (Kendall, 1977), using a method called Procrustes superimposition. The landmarks are discrete anatomical loci, selected a priori, which represent a biological structure and are homologous across individuals (Zelditch et al., 2012). The resulting shape configurations will

therefore be aligned at the origin, standardised to unit size, and rotated to the same orientation. However, fixed landmarks have the disadvantage of leaving out relevant information between landmarks, such as curvature. For this reason, sliding semi landmarks were used to analyse centrelines (Bookstein, 1997). The semi landmarks are allowed to slide along a curve to match corresponding sliding semi landmarks in the reference configuration. For this study, bending energy between the reference and target specimen was used for optimisation of the sliding process.

Landmarks

The landmarks for the SCC analysis were placed using the Amira Landmark module, on the centrelines of each canal. There were 7 landmarks placed on each specimen (2 on each canal, 1 on the common crus). For a more accurate representation of slender portion of the canals, 10 sliding landmarks were placed along the centrelines of each canal. For this, the line sets representing the centrelines were exported as coordinates and down sampled to 10 equidistant points along the entire length of each canal, using the *digit.curves* function in geomorph. A full description of the landmarks and sliding landmarks can be seen on Table 2 and Figure 1 C.

Other studies have suggested the use of an additional set of landmarks on the outer surface of each canal, in an attempt to further characterise shape changes localised closer to the centreline of the membranous labyrinth (Gunz et al., 2012). It is worth noting that when evaluating measurement error, the authors found that by changing the thresholding values and the spatial resolution of the scans, the centrelines of the canals were not affected, whilst the landmarks placed on the outer surface experienced the most variation. Given that our adult cohort comprised three datasets acquired with slightly different parameters, we opted for placing all of our landmarks along the centrelines of the canals, as to minimise potential shape changes due to differences in the scanning process. All three datasets had similar distribution in morphospace (see supplementary material for PC1 and 2 grouped by dataset). A figure of the shape configurations along PC1 and PC2 grouped by dataset is available in the supplementary material (SF1).

The GMM analysis was carried out in R (R Core Team, 2018), using the following packages: geomorph (Version 3.1.3), Morpho (Version 2.7), and RVAideMemoire (Version 4.0.3) (Schlager, 2017; Adams, Collyer and Kaliontzopoulou, 2020; Hervé, 2021).

Configuration size and shape variation

To assess the influence of size on shape, centroid size was used as a proxy. Centroid size is the square root of the sum of the squared distances between each landmark and the centroid (centre of the configuration), and it is the only measure of size that is mathematically independent of shape (Klingenberg, 2016). After testing for normality, centroid size means between adults and perinates

were compared using a T test. The medians and variances were tested using a Mood test and an F test, respectively. Procrustes distance – the square root of the sum of squared distances between corresponding Procrustes-aligned points – was used to measure the distribution of the shape configurations across the morphospace. In this instance, a value of 0 represents a shape located exactly at the mean, and increasing values represent further distance from the mean. Additionally, we performed Procrustes ANOVA to assess influence of size on shape (Goodall, 1991) and added the residuals to the mean configuration to use as size-corrected shapes. Two models were created to assess whether each group had unique or common allometries. The common allometry model was used as null model, and a Procrustes ANOVA showed no differences between the two models ($p = 0.44$), meaning the groups had a common allometric component. Principal components analysis (PCA) was used to visualise the shape variables (Procrustes-aligned coordinates) in morphospace and canonical variates analysis (CVA) was used to find maximum shape differences between the two groups. CVA analysis was performed on the first 10 PC scores after size correction. Subsequently, cross-validation was performed using leaving-one-out procedure. It is important to note that for our study, we used PCA to visualize shape changes in the GMM analysis, rather than between-group PCA (bg-PCA). Although the use of bg-PCA would have perhaps better illustrated shape differences between both groups, the decision to use PCA was made considering that bg-PCA may lead to exaggerated differences between groups that are not representative of the actual differences in the samples (Bookstein, 2019).

Measurement error

To assess repeatability of the landmarking, the semicircular canal landmarks were repeated 4 times from 5 specimens selected at random. One specimen was landmarked at a time and was not repeated until the others were completed, allowing time to pass between each specimen repeat. The repeated sets of landmarks from each specimen were submitted to generalised Procrustes alignment (GPA) and to PCA along with the rest of the samples. The repeated measurements for each specimen clustered together on the first 4 principal components, indicating small errors compared to the overall variability of the sample. PC 1 to 4 can be seen in the supplementary figures SF2 and SF3. Additionally, a Procrustes ANOVA was calculated using the individuals and repeats as categorical values. The results were then used to calculate an intraclass correlation coefficient as detailed by Fruciano (2016) which was then used to calculate repeatability. Repeatability of the landmarking was 93.4%.

SCC cross-sections

For this analysis, only 33 adults and 45 perinates were included. During preliminary tests, we found that convexity and solidity were sensitive to changes in resolution. The samples acquired at the University of Liverpool and the University of Cambridge had similar results across all metrics used for the analyses described below, whereas the Wimmer dataset fell in line with the other adults only for aspect ratio and cross-sectional area, but was an outlier for convexity and solidity (see supplementary figures S4-7). The resolution of the Wimmer dataset (60 microns) was considerably poorer than the other two (13-26 microns) and was therefore not included in the following analyses, to minimise the possibility that observed differences would be due to spatial resolution differences.

The endocast labelmaps obtained from the segmentation process and the µCT images were then re-sliced as cross-sectional images that spanned the entire length of the canals. This was done in Amira following previous literature (Johnson Chacko et al., 2018). In short, the Slice module and the Trajectory module were connected to the labels and the smoothed centreline, respectively. To iterate throughout all segments of the centreline, a tool command language (Tcl) script based on Johnson Chacko et al. (2018) was implemented. Cross-sectional images were created using the centrelines as guidelines for the slicing (Figure 1, D). The images were extracted as 2D tiff files. Additionally, a spreadsheet containing the coordinates of each point and the voxel size for each slice was generated and used for area and length calculations.

Cross-section measurements and statistical analysis

The label cross-sections were imported into ImageJ and measured using Shape Descriptors in the Measure command (1.53a v NIH, USA), and the Convex Hull option in the Edit Selection menu. The aspect ratio, solidity, convexity and cross-sectional area were used for subsequent analyses.

Aspect ratio was calculated as:

$$\frac{Major\ axis}{Minor\ axis}$$

such that 1 represents a perfect circle. Solidity and convexity are calculated by using the convex hull option in ImageJ. Solidity is calculated as

$$\frac{Area}{Convex\ Area}$$

and convexity is calculated as

$$\frac{Convex\ perimeter}{Perimeter}$$

For both solidity and convexity, values less than 1 are indicative of cross-sections with more irregular perimeters. We chose to use aspect ratio to quantify form, solidity to quantify textural roughness, and convexity to quantify morphological roughness, as defined by Liu et al. (2015). Each specimen was analysed as a stack of slices throughout the length of the canal. To perform the measurements, a script was written to iterate through each slice in the stack, select the biggest masked region (the canal) and the measurements were then performed on the selection. The area was calculated by taking the area measured in ImageJ (in pixels) and multiplied by the squared pixel size of each slice. Lastly, the lengths of the canals were calculated by summing the Euclidian distances between each point of the centrelines, as described by Johnson Chacko et al. (2018). A t test was performed to test for length differences between groups for each canal, Mood's test was performed to test for differences in the length medians, and an F test was performed to assess differences in length variances.

Resulting data points were analysed using R. Subsequent analyses for the aspect ratio, area, solidity, and convexity were performed as follows. Slice positions were standardised to percentage length, where 0 represents the beginning of the ampullated side of the canal and 100 is the point where the canal meets the vestibule, in the case of the lateral canal, or where it meets the common crus, in the case of the anterior and posterior canals. The common crus was not included in the analyses as the cross-sections were heavily influenced by the vestibule and the slender portion of the anterior and posterior canals. Then, the slices were grouped into 50 bins, as this number of provides sufficient resolution to assess canal patterns in each group. To ensure that specimens with higher resolution (more slices per bin) would not unfairly contribute to either group, measurements were averaged so that each specimen would provide one value per measurement to each bin. Afterwards, a Mann-Whitney-U test was performed for each bin to test differences between groups. Additionally, a Mood's test was performed to test for differences in the medians, and Bartlett's test was performed to assess differences in variances. We performed a Bonferroni correction of the resulting p values.

Results

Landmark analysis

Size

We found some difference in centroid sizes (Figure 2A). Adults had slightly larger centroid sizes (mean, 29.10 mm; median 29.29 mm) compared with perinates (mean, 27.84 mm; median 28.96 mm). These differences were significant (t test p-value = 0.0000497; mood's test p-value = 0.00763). indicated There was no difference in the variance of centroid size (Figure 2A) between the two groups (p = 0.739).

Shape

To visualise shape distribution in morphospace, a principal component analysis (PCA) was performed. The analysis produced 95 PCs, of which the first 25 accounted for 95% of the variance. PC 1 represents 19.01% of the variance. The distribution of the shapes between both groups overlaps on all PCs. Shape distribution along PC1 and PC2 can be seen in Figure 2C, and the shape variation along PC1 is shown in Figure 3. Most of the variation across PC1 describes relative elongation of the posterior and lateral canals, with minimal changes to the anterior canal. Individuals with the highest PC1 scores had large lateral canals and small posterior canals, whereas individuals with lower PC1 scores had large posterior and small lateral canals. We did not find any clustering of Procrustes-aligned coordinates and both groups overlapped across all PCs.

The allometric component was found to be statistically significant (p-value: 0.001), although it only accounted for 3.1% of the variation. To assess difference in morphospace distribution after size correction, the residuals from regression were added to the mean Procrustes-aligned and a PCA was conducted on these allometry-free configurations. The results from PCs 1 and 2 can be seen in Figure 2D. Unsurprisingly, the size corrected shape variables are nearly identically distributed on all major axes when compared to the original shapes.

The results for the CVA can be seen in Figure 2E. Upon cross validation, adults were only correctly classified in 66.66% of the cases, and 64.58% for the perinates (Figure 2, E and F). Lastly, the Procrustes distance from each specimen to the configuration's mean can be seen in Figure 2B. The average Procrustes distance for group were 0.067 for the adults and 0.073 for the perinates. There was no statistically significant difference between the two groups (p-value = 0.0762).

Centrelines and cross-sections

Length

The results of the lengths of the canals can be seen in Figure 4. The posterior canal was the longest of the three for both the perinatal and the adult groups. The anterior canal was the second longest, and the lateral canal was the shortest. The only canal that showed any differences in means between groups was the anterior canal, where the adults had a mean length of 14.9 mm and the perinates 14.1 mm ($p = 0.000479$), and a Mood's median test showed statistically significant differences ($p= 0. 0163$). Differences in variances were only statistically significant for the anterior canal ($p = 0.0259$), where perinates were more variable. The results for the other canals can be seen in Table 3.

Aspect ratio

We found minimal differences in aspect ratio between the two groups (Figure 5). There were no statistically significant differences in the means of the slender portion of any of the three canals. Some differences were found in the ampullary region of the lateral canal. The adults showed with aspect ratios closer to 1. The variance was also similar between both groups, except for small portions of the central region of the slender posterior and lateral canals (bins 30-40). In general, the shape of the cross sections is elliptical in both groups, but gets rounder as it approaches the vestibule on the ampullary side.

Solidity

Solidity (Figure 6) differences were more marked in the anterior canal, where they are statistically significant along almost the entire length of the slender portion. The perinatal group has solidity values closer to one than adults do, although both groups follow a very similar pattern. Differences in the posterior canal are smaller; statistically significant regions are only at the non-ampullated end of the canal, although both groups also follow similar patterns. No differences were found in the lateral canal. Notably, the perinates had a solidity closer to one across the entire length of all three canals. In general, the lowest values are at the extremes. The variance was significantly different across different sections of all three canals, although localised to specific regions of the slender portion of the canals, and in general, adults had a larger variance than perinates. Extreme examples are shown in Figure 7.

Convexity

The differences in convexity (Figure 8) were statistically significant in all three canals. The perinatal group has convexity values closer to one across the entire length of all canals. Differences were present along the entirety of all three canals, except for a few bins at the beginning of the canal in the ampullary side. The pattern of convexity is very similar between groups in the posterior and lateral canals, but diverges in the slender portion of the anterior canals, where differences were the greatest. A small portion of the lateral canal showed differences in variances (adults showed greater variance). The rest of the canals had no statistically significant difference in the amount of the variance. Extreme examples are shown in Figure 9.

Cross-sectional area

Lastly, no statistically significant differences were found for the cross-sectional area between groups in any of the canals (Figure 10). The general pattern of the area shows that the slender portion of the canal is the smallest in terms of cross-sectional area. The patterns for the anterior and lateral canals follow a parabolic shape where the area increases closer the vestibule in the ampullated and

non-ampullated sides, whereas the posterior canal is mostly flat with some increase in area at both ends. In general, both groups follow an almost identical pattern. Variance between the groups is larger for the perinates across all three canals, except for two small sections in the posterior and lateral canal, where there were no differences.

In summary, adults were only found to marginally differ from perinates in the following respects: they had slightly larger centroid sizes and slightly longer anterior semicircular canals; cross-sections from the slender portions were more elliptical and had solidity and convexity values further from one. With respect to the variability, adults were more variable than perinates in terms of canal solidity and convexity. Surprisingly, the perinates were slightly more variable than the adults in terms of cross-sectional area and anterior canal length. In all other respects, adults were not different to perinates.

Discussion

For this study, we set out to test the hypothesis that bone remodelling disinhibition in perilabyrinthine bone can lead to changes and/or increased variation in the shape and the size of the bony semicircular canals during postnatal life. The disinhibition of bone remodelling would allow for new bone formation and bone resorption on the surface of the bony labyrinth, which could be organised or stochastic. In the former, we would expected to see significant differences in the shape and size of the canals between perinates and adults, both in the overall canal configuration and in the anatomy of individual canals. Such changes could reflect functional shifts, possibly the maturation of obligatory bipedalism. For stochastic change, we expected that size or shape may not differ, but that the adult cohort would exhibit greater variation than the perinates, following bone remodelling disinhibition.

We observed several metrics where directional change had occurred. One such change is in size. We set out to evaluate size by looking at three different metrics: the centroid size of the landmark configuration shape, the length of the canals and finally, their cross-sectional area. The results supported our hypothesis that size of the canals is different between the two groups to limited extent. We found that adults have on average a larger centroid size and a longer anterior canal. Differences, however, only represented around 4.4% change in centroid size and the lengthening of the anterior canal was only around 4.6%. To put this in context, the largest adult centroid size was 22.5% larger than the smallest adult centroid size. Additionally, we found almost no differences in cross-sectional area, aside from a small portion of the posterior canal. A previous study suggests that humans achieve adult semicircular canal size in utero, around the 18th week of gestational age (Jeffery and Spoor, 2004). Findings from the current study suggest there is a subtle size change after

birth. The longer anterior canal corroborates other reports of differences in size due to lengthening of the canals with increases as much as 3 mm (Tremble, 1929). However, Daocai et al. (2014) measured the length and width of each canal in young children (<7yrs) as well as adults and found no statistically significant differences. The authors used a single plane that most optimally displayed the entirety of the semicircular canal. It is possible, therefore, that measurements could have been skewed due to the torsion of semicircular canals that has been reported (see Sato et al., 1993; Ifediba et al., 2007). It is also possible that Daocai et al. averaged out changes by aggregating findings from 9 months to 7 years in their young children category. The average area for the slender portion of the adult canals reported here was also similar to that for adult humans reported by Johnson Chacko et al. (2018), both in terms of size at around 0.8 to 1.2 mm2 and the pattern of variation along the canal. The parabolic distribution of the cross-sectional area is due to the widening of the canals at the ampulla and the transition from slender portion to the wider vestibule. It should be noted that determining centrelines seemed less reliable near the vestibule and the common crus, where the skeletonization process would have included parts of the vestibule as well as the canal, and probably exaggerated the corresponding aspect ratios and cross-sectional areas. In summary, there was limited evidence for small scale (<5%) size change after birth but we do not envisage these to be functionally significant. Moreover, we cannot discount sampling or measurement error biases with respect to such small margins.

In terms of shape, organised changes were less consistent. Configuration shape, for example, was similar in perinates and adults. The trend across PC1 for both age groups described a relative lengthening of the posterior and lateral canals, with minimal changes to the anterior canal. These results seem to contradict our findings regarding lengthening of the anterior canal. This is because the lengths of the posterior and lateral canal were more variable overall compared to the anterior canal (see coefficients of variation in Table 3), but were more similarly distributed across both adults and perinates. By contrast, the overall range of variation smaller for the anterior canal, but the distribution (and the mean) was different when comparing adults and perinates (see Figure 4). When considering the shape changes along PC1, it is also important to bear in mind that these were not representative of a single group, rather the variation across our entire sample (perinates and adults together). Shape measures representing the canal cross-section painted a slightly different picture. Aspect ratio, for example, showed differences between groups in the posterior and lateral canals. In both groups, nonetheless, the slender portion of the canals was elliptical, which is consistent with previous reports (Ifediba et al., 2007). By contrast, the measures of solidity and convexity were generally further away from unity in adults, which is indicative of increased irregularity for the internal walls of the bony canals. Broadly, our results showed little organised difference of bony

canal shape between perinates and adults. This would seem to support the notion of its functional imperativeness necessitating tighter genetic regulation of form, which in turn supports previous studies showing a close correspondence of form with, for example, population genetics (Ponce de León et al., 2018).

Some evidence of heighten variation was also detected between our groups. Whilst there were no differences in the variability of the configuration size (centroid size), we did find that perinates have a more variable anterior canal length compared to adults. This is not consistent with our hypothesis that postnatal disinhibition heralds disordered changes to the bony canal. Adults did have more variable convexity and solidity measures than perinates, especially in the anterior canal, and more variable aspect ratios in some sections of the slender portion as well. It is tempting to suggest that this proves the disinhibition of bone remodelling. However, it is important to note that solidity and convexity measures will have been sensitive to thresholding and interpolation artefacts. In addition, adult variability may also have been exaggerated by the inevitable limitations of our samples. Human material is scarce and therefore the adult group was drawn from several sources to achieve reasonable N values. Unfortunately, the metadata available for these different sources were patchy. We do not know, for example, the exact ages of the adult Liverpool and Wimmer dataset specimens, nor the gender of any of the adults. Consequently, the greater adult variation may be due in part to, for example, differences of ageing, in particular age and gender related oestrogen levels, and other environmental factors that we cannot attribute given the paucity of biometric data available. By contrast, the perinatal cohort was geographically, ontogenetically and chronologically confined, and whilst the causes of premature death were unknown and could have included, for example, malnutrition, recent work on rats suggests that the inner ear remains relatively imperious such factors (Ward et al., 2021). Thus, our data only infers and cannot prove that the adult bony canals were disinhibited in comparison with perinates. Similarly, it is also possible that noise within the populations masked subtler size or shape differences consistent with co-ordinated bone remodelling. Further investigation is thus warranted using, for example, histological techniques to validate microCT data captured for more widely available non-human animal material.

Overall, our findings seem to suggest that the remaining osteocytes are sufficient to supress substantive postnatal size and shape change. This implies that functional changes linked to postural maturation and the transition to bipedalism, which is not completed until around 15 months of age, are predominantly, if not entirely, accommodated by postnatal adjustments of the underlying neurophysiological systems (Ornitz et al., 1979; Dechesne and Sans, 1985). But if the early bony form is good enough and that, for example, the vestibular pathways can be relied upon to adapt the signal encoding to accommodate a range of functions, why inhibit bone remodelling and constrain that

bony form in the first place? A possible explanation is that we are looking in the wrong place for the associated form changes. In our study, we could only examine bony labyrinths. It is possible that postnatal functionally related adjustments are reflected more so in the morphology of the membranous labyrinth, where signal mechanotransduction occurs. The membranous part adheres to the outermost internal surface of the bony canal and the lengths should be closely correlated. It may therefore be the case that bony morphology is constrained to maintain the length of the membranous canals within certain tolerances. Indeed, we may have understated the potential importance of the small but significant postnatal increase in the length of the bony, and presumably of the membranous, anterior semicircular canal, which is particularly sensitive to movements in the vertical plane and whose lengthening has been linked to the evolution of human bipedalism (Spoor et al., 1994; Fitzpatricket al., 2006). In addition, there is scope for form-function modifications of the cross-sectional geometry of the membranous canal to go unnoticed because it occupies less than 10% of the bony canal lumen with the remaining space filled with perilymph and a fibroblast trabeculae (Curthoys et al.1977). In humans the space forms rapidly in-utero and lines the full length of each membranous canal by around 13 weeks in-utero (Ishikawa et al., 2018). Remarkably, the role of this space remains elusive with several theories falling foul of observations of its microanatomical structure and incidence among extant taxa of varying body sizes, phylogenies and modes of locomotion (Gray, 1908; Curthoys, Markham and Curthoys, 1977). Clearly, more ontogenetic and comparative work is warranted to investigate the life-course extent or limit of phenotypic plasticity of the membranous canal in relation to its bony counterpart.

Conclusions

Our study highlights diminutive changes of canal size (centroid size and anterior canal length) but no notable differences of overall shape nor increased variability in these parameters amongst adults. Differences in variance observed in the cross-sectional shape of the canals tentatively support our hypothesis of entropic disinhibition of bone remodelling among adults, although whole labyrinth variance was not different from perinates. In general, the overall shape and the ellipsoidal cross-sectional shape of the slender portion of the canals is achieved prenatally and conserved through life. That the bony canals form so early during development and seemingly remain impervious to functional milestones such as the maturation of obligatory bipedalism seems extraordinary.

Acknowledgements

We would like to thank William Ashley-Fenn and Dr Matthew J. Mason for sharing microCT data for our project. Thanks to Dominik Thomas Schmidbauer for kindly walking us through his original code for re-slicing the canals in Amira.

Author contributions

Cárdenas-Serna, M

Data acquisition, data analysis, data interpretation, drafting of the manuscript.

Jeffery, N

Data acquisition, drafting of the manuscript, critical revision of the manuscript.

References

Adams, D. C., Collyer, M. L. and Kaliontzopoulou, A. (2020) 'Geomorph: Software for geometric morphometric analyses. R package version 3.2.1.' Available at: https://cran.r-project.org/package=geomorph.

Berlin, J. C., Kirk, E. C. and Rowe, T. B. (2013) 'Functional implications of ubiquitous semicircular canal non-orthogonality in mammals', PLoS One, 8(11), p. e79585. doi: https://doi.org/10.1371/journal.pone.0079585.

Blanks, R. H. et al. (1985) 'Planar relationships of the semicircular canals in rhesus and squirrel monkeys', Brain research, 340(2), pp. 315–324.

Bloch, S. L., Kristensen, S. L. and Sørensen, M. S. (2012) 'The Viability of Perilabyrinthine Osteocytes: A Quantitative Study Using Bulk-Stained Undecalcified Human Temporal Bones', The Anatomical Record, 295(7), pp. 1101–1108. doi: 10.1002/ar.22492.

Bloch, S. L. and Sørensen, M. S. (2010) 'The viability and spatial distribution of osteocytes in the human labyrinthine capsule: A quantitative study using vector-based stereology', Hearing Research, 270(1), pp. 65–70. doi: 10.1016/j.heares.2010.09.007.

Bookstein, F. L. (1991) Morphometric tools for landmark data: geometry and biology. Cambridge University Press.

Bookstein, F. L. (1996) 'Biometrics, biomathematics and the morphometric synthesis', Bulletin of Mathematical Biology, 58(2), pp. 313–365. doi: 10.1007/BF02458311.

Bookstein, F. L. (1997) ‘Landmark methods for forms without landmarks: morphometrics of group differences in outline shape’, Medical Image Analysis, 1(3), pp. 225–243. doi: 10.1016/s1361-8415(97)85012-8.

Bookstein, F. L. (2019) ‘Pathologies of Between-Groups Principal Components Analysis in Geometric Morphometrics’, Evolutionary Biology, 46(4), pp. 271–302. doi: 10.1007/s11692-019-09484-8.

Cox, P. G. and Jeffery, N. (2010) ‘Semicircular canals and agility: the influence of size and shape measures’, Journal of Anatomy, 216(1), pp. 37–47. doi: doi: 10.1111/j.1469-7580.2009.01172.x.

Curthoys, I. S., Markham, C. H. and Curthoys, E. J. (1977) ‘Semicircular duct and ampulla dimensions in cat, guinea pig and man’, Journal of Morphology, 151(1), pp. 17–34. doi: 10.1002/jmor.1051510103.

Daocai, W. et al. (2014) ‘Size of the Semicircular Canals Measured by Multidetector Computed Tomography in Different Age Groups’:, Journal of Computer Assisted Tomography, 38(2), pp. 196–199. doi: 10.1097/RCT.0b013e3182aaf21c.

David, R. et al. (2010) ‘Motion from the past. A new method to infer vestibular capacities of extinct species’, Comptes Rendus Palevol, 9(6), pp. 397–410. doi: 10.1016/j.crpv.2010.07.012.

Fitzpatrick, R. C., Butler, J. E. and Day, B. L. (2006) ‘Resolving Head Rotation for Human Bipedalism’, Current Biology, 16(15), pp. 1509–1514. doi: 10.1016/j.cub.2006.05.063.

Frisch, T. et al. (2000) ‘Estimation of volume referent bone turnover in the otic capsule after sequential point labeling’, Annals of Otology, Rhinology & Laryngology, 109(1), pp. 33–39.

Fruciano, C. (2016) ‘Measurement error in geometric morphometrics’, Development Genes and Evolution, 226(3), pp. 139–158. doi: 10.1007/s00427-016-0537-4.

Goodall, C. (1991) ‘Procrustes Methods in the Statistical Analysis of Shape’, Journal of the Royal Statistical Society. Series B (Methodological), 53(2), pp. 285–339.

Goyens, J. (2019) ‘High ellipticity reduces semi-circular canal sensitivity in squamates compared to mammals’, Scientific Reports, 9(1), p. 16428. doi: 10.1038/s41598-019-52828-9.

Gray, A. A. (1908) The labyrinth of animals: including mammals, birds, reptiles and amphibians. J. & A. Churchill.

Gunz, P. et al. (2012) ‘The mammalian bony labyrinth reconsidered, introducing a comprehensive geometric morphometric approach.’, Journal of anatomy, 220(6), pp. 529–543. doi: 10.1111/j.1469-7580.2012.01493.x.

Hervé, M. (2021) RVAideMemoire: Testing and plotting procedures for biostatistics. manual. Available at: https://CRAN.R-project.org/package=RVAideMemoire.

Ifediba, M. A. et al. (2007) 'The role of 3-canal biomechanics in angular motion transduction by the human vestibular labyrinth.', Annals of biomedical engineering, 35(7), pp. 1247–1263. doi: 10.1007/s10439-007-9277-y.

Ishikawa, A. et al. (2018) 'Formation of the Periotic Space During the Early Fetal Period in Humans', The Anatomical Record, 301(4), pp. 563–570. doi: https://doi.org/10.1002/ar.23764.

Iversen, M. M. and Rabbitt, R. D. (2017) 'Wave Mechanics of the Vestibular Semicircular Canals', Biophysical Journal, 113(5), pp. 1133–1149. doi: 10.1016/j.bpj.2017.08.001.

Jeffery, N. and Spoor, F. (2004) 'Prenatal growth and development of the modern human labyrinth.', Journal of anatomy, 204(2), pp. 71–92. doi: 10.1111/j.1469-7580.2004.00250.x.

Johnson Chacko, L. et al. (2018) 'Analysis of Vestibular Labyrinthine Geometry and Variation in the Human Temporal Bone', Frontiers in Neuroscience, 12. doi: 10.3389/fnins.2018.00107.

Jones, G. M. and Spells, K. (1963) 'A theoretical and comparative study of the functional dependence of the semicircular canal upon its physical dimensions', Proceedings of the Royal Society of London. Series B. Biological Sciences, 157(968), pp. 403–419.

Kendall, D. G. (1977) 'The diffusion of shape', Advances in Applied Probability, 9(3), pp. 428–430. doi: 10.2307/1426091.

Klingenberg, C. P. (2016) 'Size, shape, and form: concepts of allometry in geometric morphometrics', Development Genes and Evolution, 226(3), pp. 113–137. doi: 10.1007/s00427-016-0539-2.

Lambert, F. M. et al. (2008) 'Semicircular Canal Size Determines the Developmental Onset of Angular Vestibuloocular Reflexes in Larval Xenopus', The Journal of Neuroscience, 28(32), pp. 8086–8095. doi: 10.1523/JNEUROSCI.1288-08.2008.

Le Maitre, A. et al. (2017) 'New data about semicircular canal morphology and locomotion in modern hominoids.', Journal of anatomy, 231(1), pp. 95–109. doi: 10.1111/joa.12619.

Lee, J.-Y. et al. (2013) 'A Morphometric Study of the Semicircular Canals Using Micro-CT Images in Three-Dimensional Reconstruction', The Anatomical Record, 296(5), pp. 834–839. doi: 10.1002/ar.22664.

Liu, E. J., Cashman, K. V. and Rust, A. C. (2015) 'Optimising shape analysis to quantify volcanic ash morphology', GeoResJ, 8, pp. 14–30. doi: 10.1016/j.grj.2015.09.001.

556 Muren, C., Ruhn, G. and Wilbrand, H. (1986) 'Anatomic Variations of the Human Semicircular Canals:
557 A Radioanatomic Investigation', Acta Radiologica. Diagnosis, 27(2), pp. 157–163. doi:
558 10.1177/028418518602700205.

559 Obrist, D. (2019) 'Flow Phenomena in the Inner Ear', Annual Review of Fluid Mechanics, 51(1), pp.
560 487–510. doi: 10.1146/annurev-fluid-010518-040454.

561 Ornitz, E. M. et al. (1979) 'The Maturation of Vestibular Nystagmus in Infancy and Childhood', Acta
562 Oto-Laryngologica, 88(1–6), pp. 244–256. doi: 10.3109/00016487909137166.

563 Ponce de León, M. S. et al. (2018) 'Human bony labyrinth is an indicator of population history and
564 dispersal from Africa', Proceedings of the National Academy of Sciences, 115(16), pp. 4128–4133.
565 doi: 10.1073/pnas.1717873115.

566 R Core Team (2018) R: A Language and Environment for Statistical Computing. Vienna, Austria: R
567 Foundation for Statistical Computing. Available at: https://www.R-project.org/.

568 Rabbitt, R. D. (1999) 'Directional coding of three-dimensional movements by the vestibular
569 semicircular canals', Biological Cybernetics, 80(6), pp. 417–431. doi: 10.1007/s004220050536.

570 Rabbitt, R. D., Damiano, E. R. and Grant, J. W. (2004) 'Biomechanics of the semicircular canals and
571 otolith organs', in The vestibular system. Springer, pp. 153–201.

572 Ryan, T. M. et al. (2012) 'Evolution of locomotion in Anthropoidea: the semicircular canal evidence',
573 Proceedings of the Royal Society B: Biological Sciences, 279(1742), pp. 3467–3475. doi:
574 10.1098/rspb.2012.0939.

575 Sato, H. et al. (1993) 'Torsion of the Human Semicircular Canals and its Influence on their Angular
576 Relationships', Acta Oto-Laryngologica, 113(2), pp. 171–175. doi: 10.3109/00016489309135787.

577 Schlager, S. (2017) 'Morpho and rvcg – shape analysis in R', in Zheng, G., Li, S., and Szekely, G. (eds)
578 Statistical shape and deformation analysis. Academic Press, pp. 217–256.

579 Spoor, F. et al. (2007) 'The primate semicircular canal system and locomotion', Proceedings of the
580 National Academy of Sciences, 104(26), pp. 10808–10812.

581 Spoor, F., Wood, B. and Zonneveld, F. (1994) 'Implications of early hominid labyrinthine morphology
582 for evolution of human bipedal locomotion', Nature, 369(6482), pp. 645–648. doi:
583 10.1038/369645a0.

584 Spoor, F. and Zonneveld, F. (1995) 'Morphometry of the primate bony labyrinth: a new method
585 based on high-resolution computed tomography.', Journal of Anatomy, 186(Pt 2), pp. 271–286.

586 Spoor, F. and Zonneveld, F. (1998) ‘Comparative review of the human bony labyrinth’, American
587 Journal of Physical Anthropology: The Official Publication of the American Association of Physical
588 Anthropologists, 107(S27), pp. 211–251.

589 Tremble, G. E. (1929) ‘THE BONY LABYRINTH OF THE NEW-BORN INFANT AND OF THE ADULT: A
590 COMPARATIVE STUDY’, Archives of Otolaryngology - Head and Neck Surgery, 9(2), pp. 175–180. doi:
591 10.1001/archotol.1929.00620030189006.

592 Van Buskirk, W. C. (1988) ‘The biomechanics of the semicircular canals’, in. Proceedings of the
593 Annual International Conference of the IEEE Engineering in Medicine and Biology Society, IEEE, pp.
594 1056–1057.

595 Walker, A. et al. (2008) ‘The semicircular canal system and locomotion: the case of extinct lemuroids
596 and lorisoids’, Evolutionary Anthropology: Issues, News, and Reviews: Issues, News, and Reviews,
597 17(3), pp. 135–145.

598 Ward, D. L. et al. (2021) ‘Early life malnutrition and fluctuating asymmetry in the rat bony labyrinth’,
599 The Anatomical Record, n/a(n/a). doi: https://doi.org/10.1002/ar.24601.

600 Wimmer, W. et al. (2019) ‘Human Bony Labyrinth: Co-Registered CT and micro-CT Images, Surface
601 Models and Anatomical Landmarks’. doi: 10.5281/zenodo.3355272.

602 Yang, A. and Hullar, T. E. (2007) ‘Relationship of semicircular canal size to vestibular-nerve afferent
603 sensitivity in mammals’, Journal of neurophysiology, 98(6), pp. 3197–3205.

604 Zehnder, A. F. et al. (2005) ‘Osteoprotegerin in the Inner Ear May Inhibit Bone Remodeling in the
605 Otic Capsule’, The Laryngoscope, 115(1), pp. 172–177. doi: 10.1097/01.mlg.0000150702.28451.35.

606 Zelditch, M. L., Swiderski, D. L. and Sheets, H. D. (2012) Geometric morphometrics for biologists: a
607 primer. Academic Press.

608

609 Tables

610 *Table 1: Samples details by group and dataset. Further information on each of the specimens is available as a supplementary*
611 *table.*

Group – dataset	Age (years)	Sex & N	Spatial resolution (µm)	Configuration analysis	Cross-sectional analysis

Perinates – Liverpool	< 0.5	Female: 6 Male: 9 Unknown: 33	~13	Yes	Yes
Adult – Liverpool	Unknown	Unknown: 17	~ 13	Yes	Yes
Adult – Cambridge	68 to 98	Unknown: 16	~ 25	Yes	Yes
Adult – Wimmer	Unknown	Unknown: 15	~ 61	Yes	No

612

613 *Table 2: SCC landmarks and description. All landmarks are placed on the centrelines generated by the skeletonization*
614 *process.*

Canal	No.	Landmark description	Landmark type
Anterior (ASC)	1	Centre of the ampulla of the ASC	Fixed
	2	Slender portion of the canal meets the ampulla	Fixed
Posterior (PSC)	3	Centre of the ampulla of the PSC	Fixed
	4	Slender portion of the canal meets the ampulla	Fixed
Lateral (LSC)	5	Centre of the ampulla of the LSC	Fixed
	6	Slender portion of the canal meets the ampulla	Fixed
Common crus (CC)	7	Common crus as it meets the vestibule	Fixed
ASC	8	Anchor anterior (ampullated side meets vestibule)	Fixed
	9-18	10 equidistant points across the canal.	Sliding
	19	Anchor anterior (common crus bifurcation)	Fixed
PSC	20	Anchor posterior (ampullated side meets vestibule)	Fixed
	21-30	10 equidistant points across the canal.	Sliding
	19	Anchor posterior (common crus bifurcation)	Fixed
LSC	31	Anchor lateral (ampullated side meets vestibule)	Fixed
	32-41	10 equidistant points across the canal.	Sliding
	42	Anchor lateral (non-ampullated side meets vestibule)	Fixed

615

616 *Table 3: Semicircular canal length mean, median and coefficient of variation. Perinates and adults are compared using a t-*
617 *test (difference of means), a Mood's test (difference of medians), and an F test (difference in variation).*

Canal	Mean (mm)			Median (mm)			Coefficient of variation		
	Adult	Perinate	P value	Adult	Perinate	P value	Adult	Perinate	P value
Anterior	14.867	14.107	**0.000479**	14.962	14.181	**0.0163**	0.0531	0.0804	**0.0259**
Posterior	16.025	16.182	0. 656	16.299	16.242	0.828	0.106	0.0912	0.361
Lateral	12.322	11.862	0.0518	12.335	11.984	0.050	0.080	0.0983	0.305

Figures

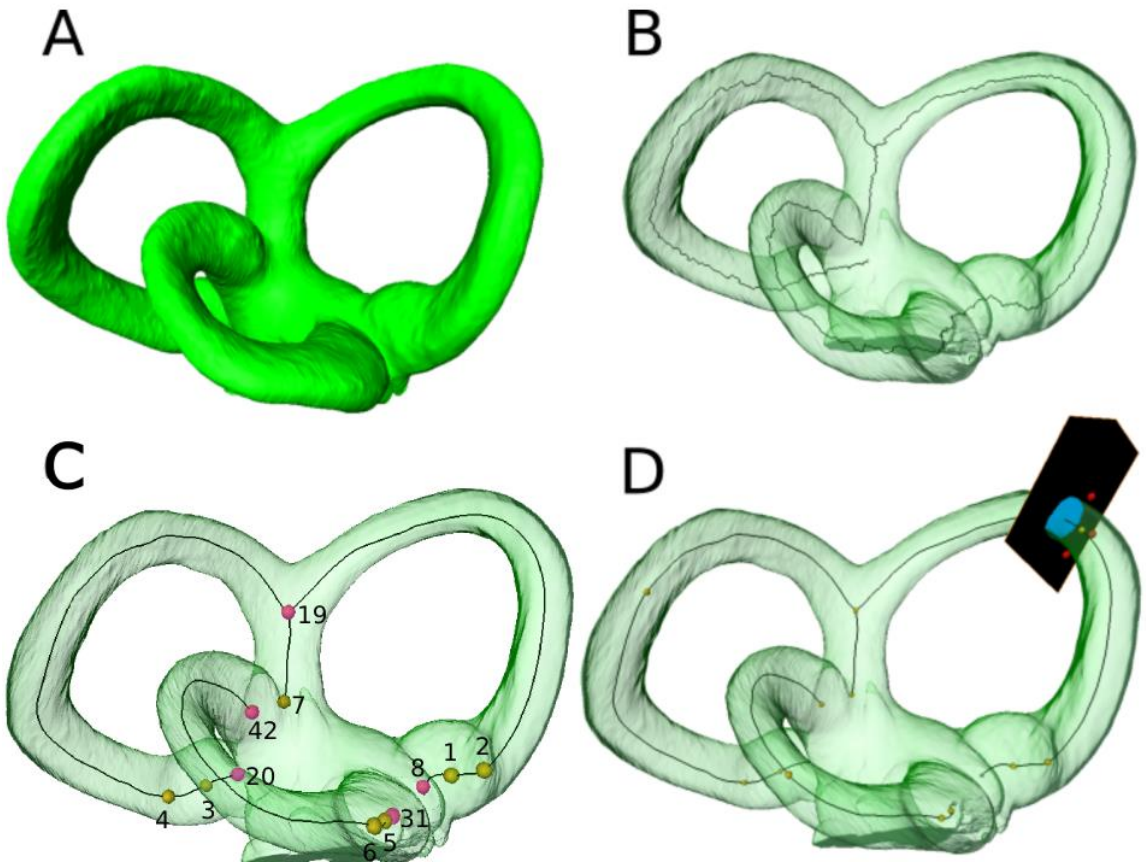

Figure 1: Segmentation of the SCC endocasts to calculate centrelines. A: A surface map generated from a completed segmentation of the three canals and the superior portion of the vestibule. B: Centrelines calculated using the skeletonization procedure (distance ordered thinner and trace lines). C: Centrelines are smoothed and cropped at the points where the canals meet the vestibule. Landmarks are placed along the centreline of the canals. In yellow: fixed landmarks. In pink: fixed landmarks used as anchors for sliding landmarks. D: the centrelines are used to generate perpendicular slices along the length of the canals. Section in blue represents the segmented bony canal, which is then used for the analyses.

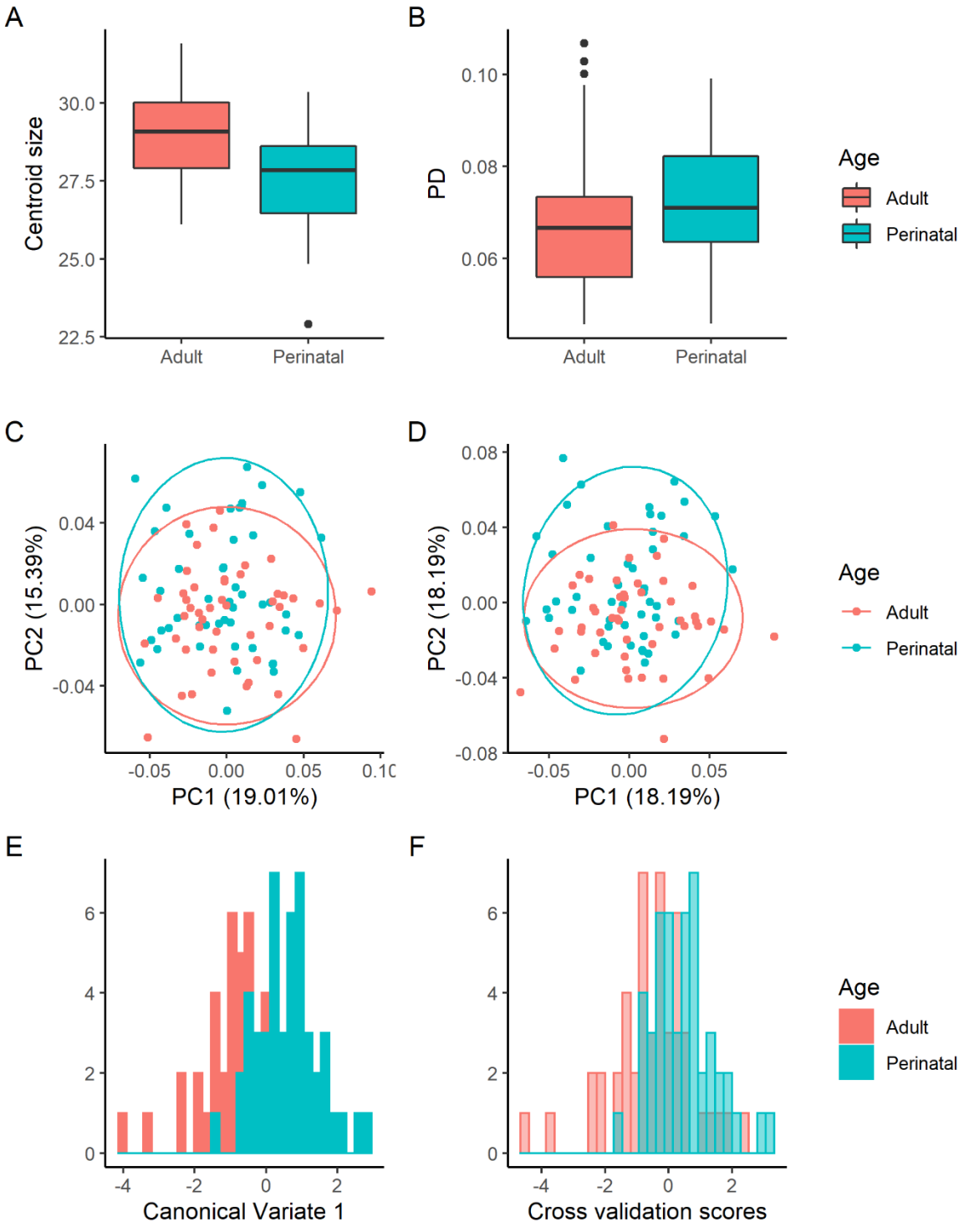

627

628 *Figure 2: GMM analysis of SCC. A: Centroid size by age group (mm). B: Procrustes distance (PD) from shape*
629 *configuration mean by group. C: PCA (PCs 1 and 2) from original shape variables. D: PCA (1 and 2) of allometry-corrected*
630 *shapes. PCA plots show 90% confidence ellipses of population means. E: Canonical variate 1 by age group. F: Cross*
631 *validation scores from CVA using leave-one-out procedure.*

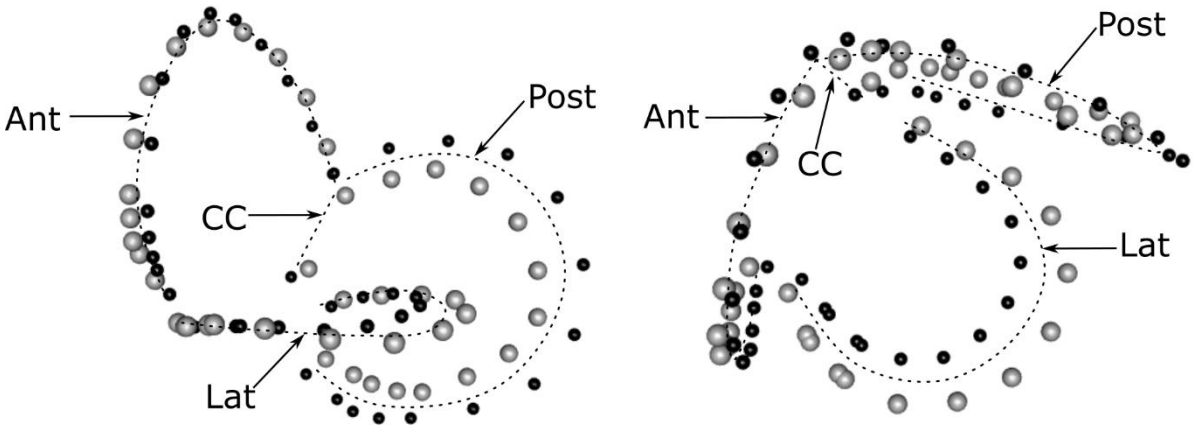

Figure 3: Shape changes along principal component 1. Black dots represent extreme values at PC1 min, and grey dots represent extreme values at PC1 max. Dotted lines illustrate general shape of the canals for ease of visualisation. The greatest changes are seen in the size of the posterior and lateral canals, with minimal changes to the anterior canal. NB these changes do not represent actual specimens, and neither group localised to a particular region of PC1.

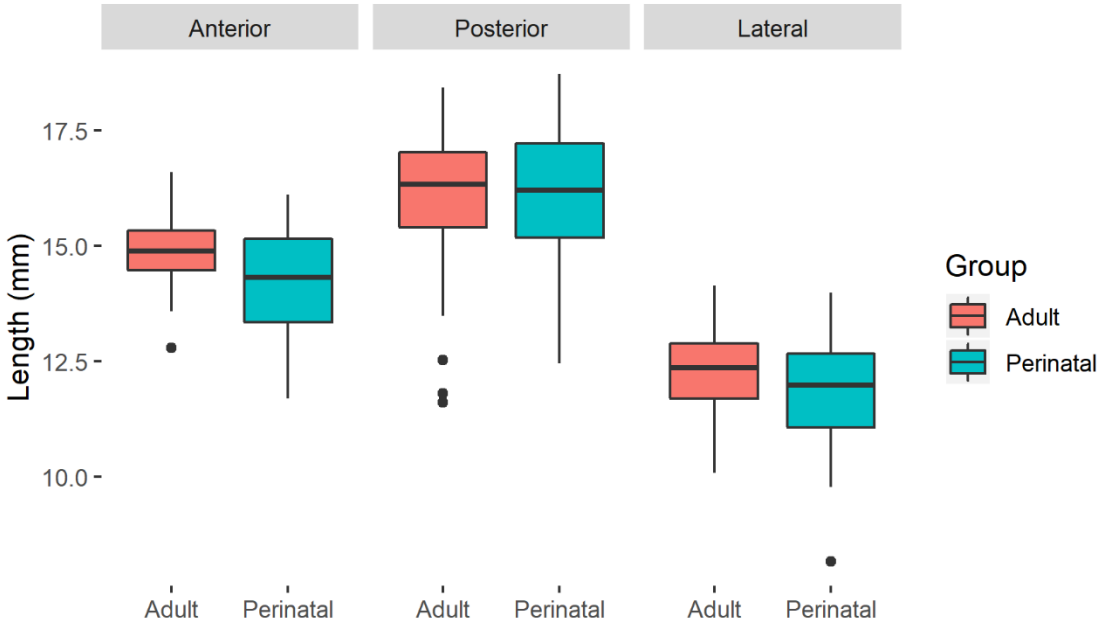

Figure 4: Centreline length. Lengths were calculated by computing Euclidian distances between each point in the centreline of the canals. Centrelines were trimmed at the point where each canal met the vestibule and/or the common crus. Only the anterior canal showed significant differences between group means and medians (Refer to Table 3).

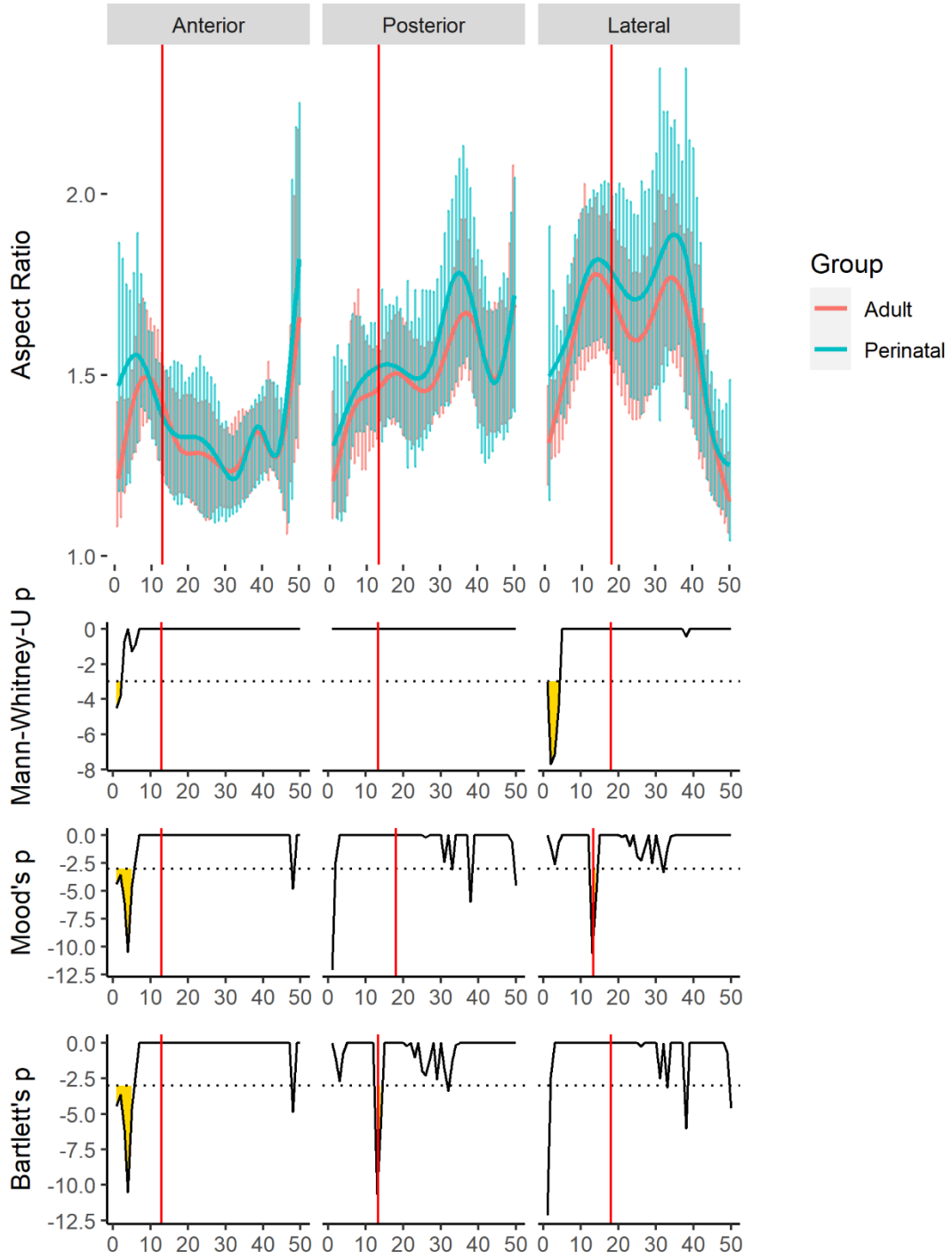

641

642 *Figure 5: Aspect Ratio. Each canal represented by 50 bins, which span the length of the canal, from the ampulla to the*
643 *vestibule or the common crus. Vertical red lines represent the average ampulla start. Top: Solid lines represent the smoothed*
644 *mean for each group. Vertical coloured lines are the standard deviations each group bin. Bottom: log p values for Mann-*
645 *Whitney-U, Mood's and Bartlett tests for differences between adult and perinate bin means, medians and variances,*
646 *respectively. Horizontal dotted line represents log 0.05 and yellow area under the curve highlights bins with statistically*
647 *significant differences (p<0.05).*

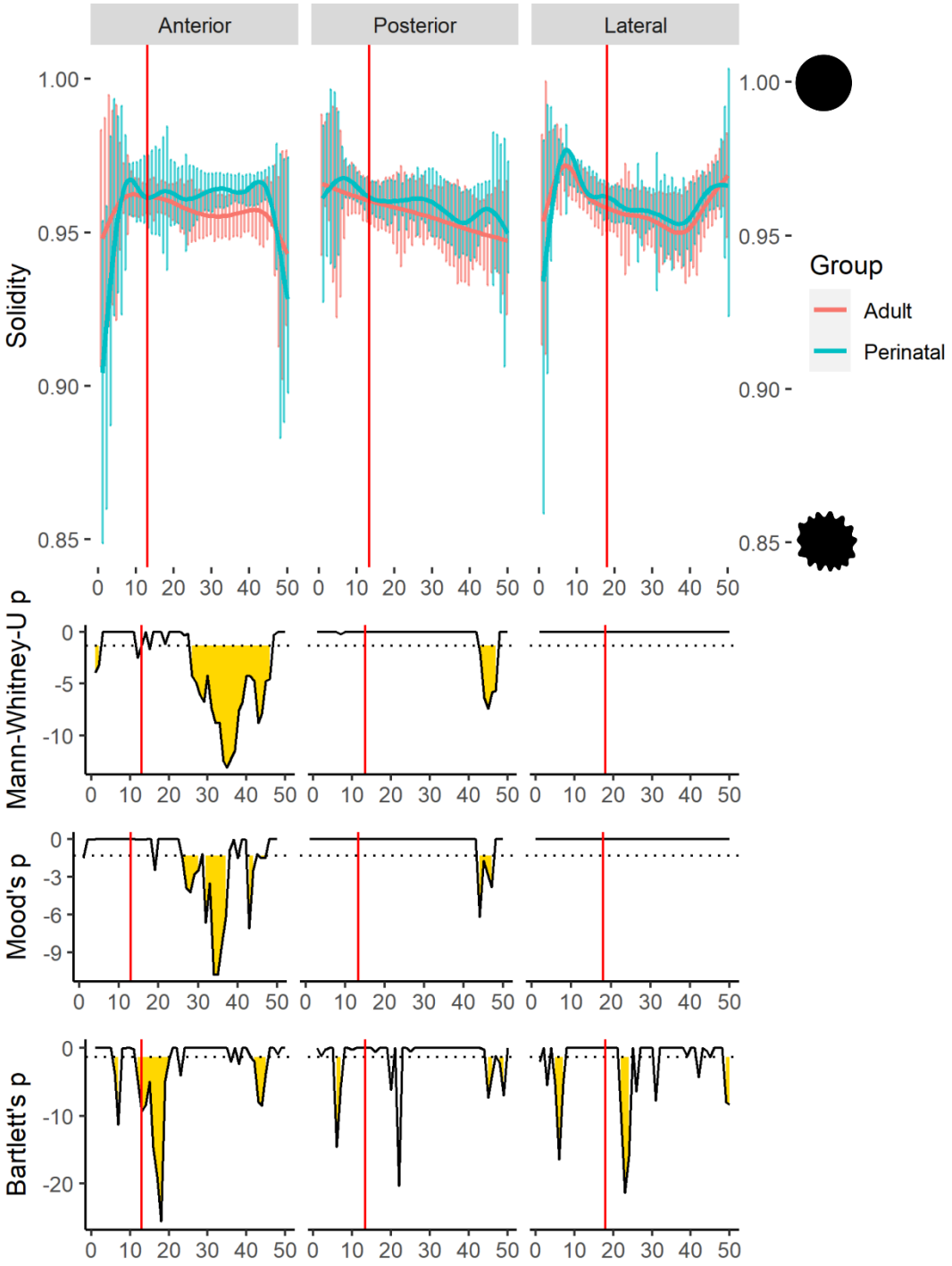

Figure 6: Solidity. Each canal represented by 50 bins, which span the length of the canal, from the ampulla to the vestibule or the common crus. Vertical red lines represent the average ampulla start. Top: Solid lines represent the smoothed mean for each group. Vertical coloured lines are the standard deviation for each group bin. Bottom: log p values for Mann-Whitney-U, Mood's and Bartlett tests for differences between adult and perinate bin means, medians and variances, respectively. Horizontal dotted line represents log 0.05 and yellow area under the curve highlights bins with statistically significant differences ($p<0.05$).

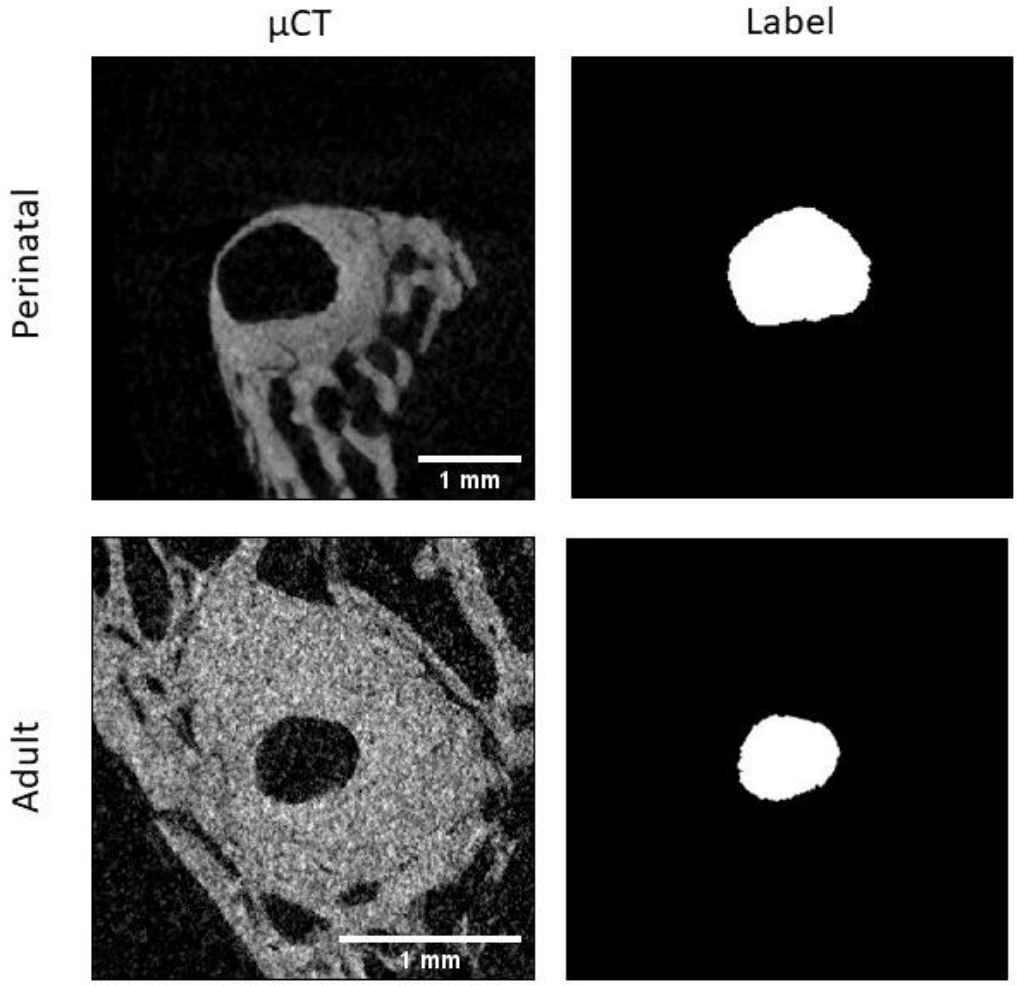

655

656 *Figure 7: microCT and labelmap of an adult and perinatal specimen at bin 35 of the anterior canal. The solidity measures*
657 *were 0.96 and 0.95 for the perinatal and adult, respectively.*

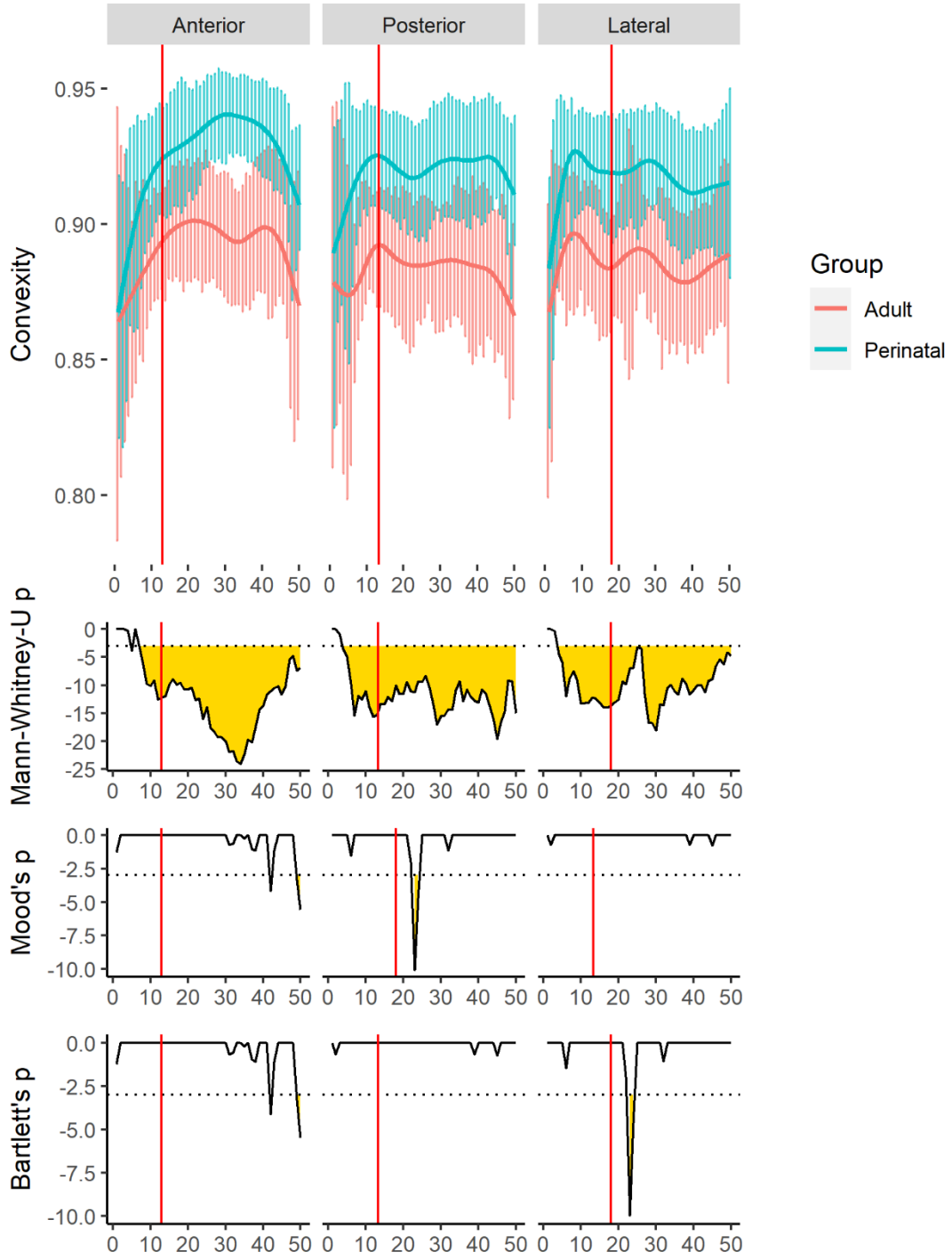

Figure 8: Convexity. Each canal represented by 50 bins, which span the length of the canal, from the ampulla to the vestibule or the common crus. Vertical red lines represent the average ampulla start. Top: Solid lines represent the smoothed mean for each group. Vertical coloured lines are the standard deviation each group bin. Bottom: log p values for Mann-Whitney-U, Mood's and Bartlett tests for differences between adult and perinate bin means, medians and variances, respectively. Horizontal dotted line represents log 0.05 and yellow area under the curve highlights bins with statistically significant differences ($p<0.05$).

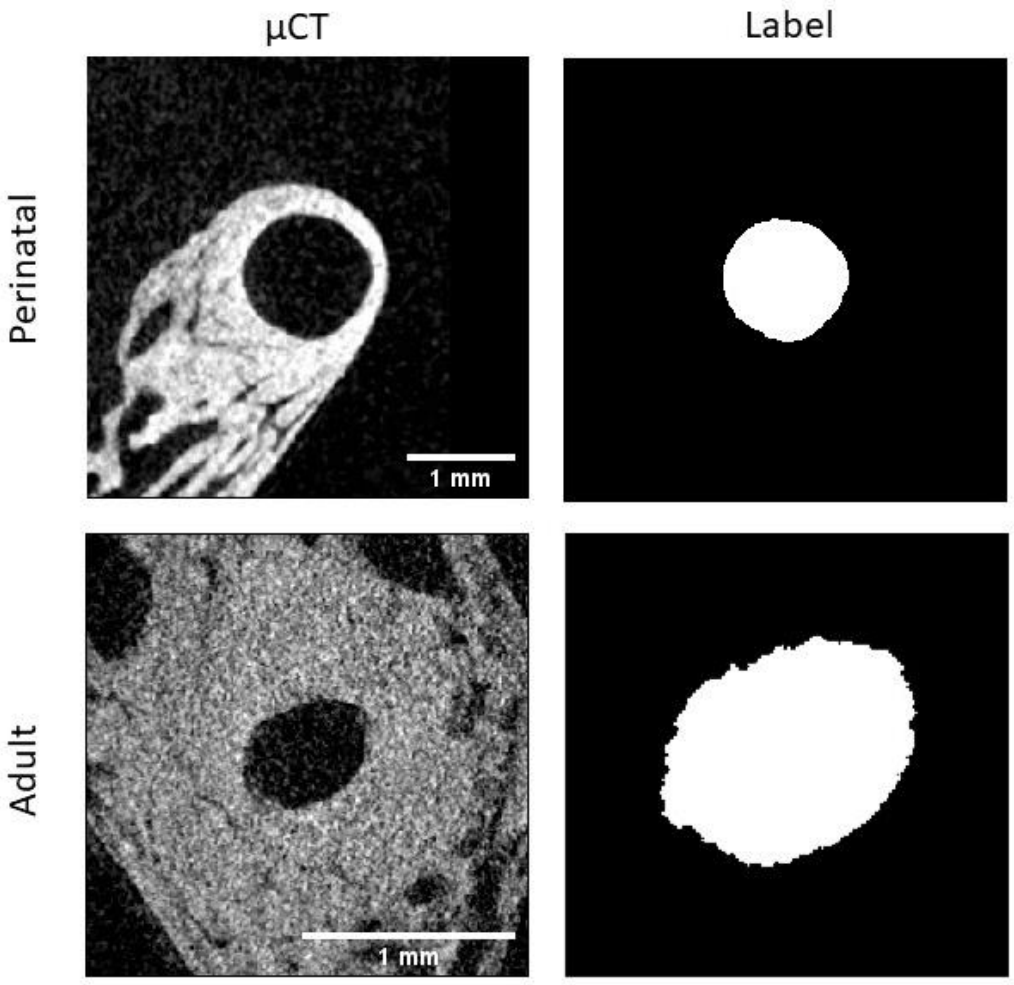

665

666 *Figure 9: microCT and labelmap of an adult and perinatal specimen at bin 30 of the anterior canal. The convexity measures*
667 *were 0.97 and 0.86 for the perinatal and adult, respectively.*

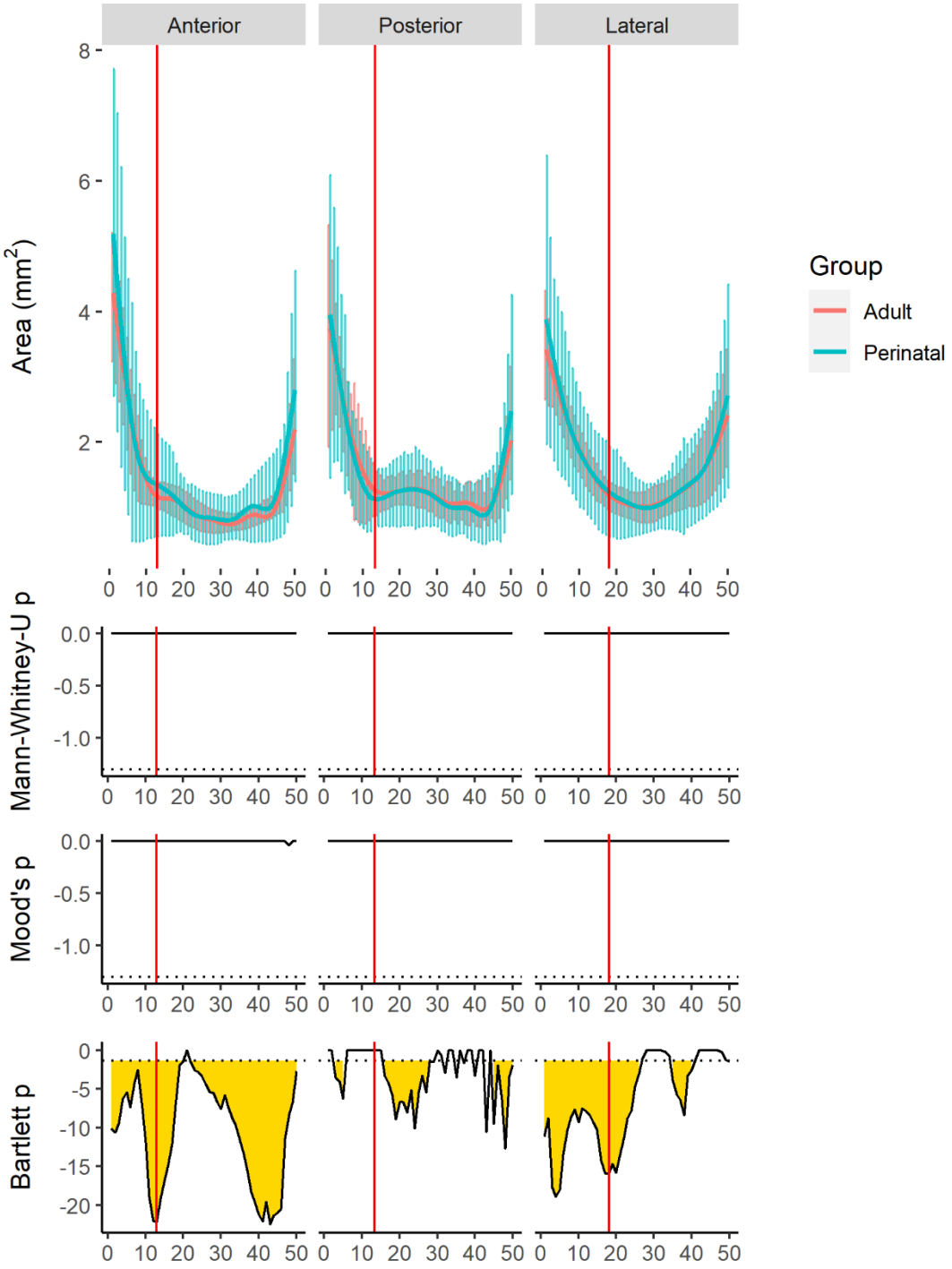

Figure 10: Cross-sectional area. Each canal is shown in 50 different bins, which represent the length of the canal, from the ampulla to the vestibule or the common crus. Vertical red lines represent the average ampulla start. Top: Solid lines represent the smoothed mean for each group. Vertical coloured lines are the standard deviation each group bin. Bottom: log p values for Mann-Whitney-U, Mood's and Bartlett tests for differences between adult and perinate bin means, medians and variances, respectively. Horizontal dotted line represents log 0.05 and yellow area under the curve highlights bins with statistically significant differences ($p<0.05$).

Supplementary material

The raw landmark data and the cross-sectional measures for all specimens in this study can be found at https://doi.org/10.5281/zenodo.4818568 .

Supplementary Figures captions

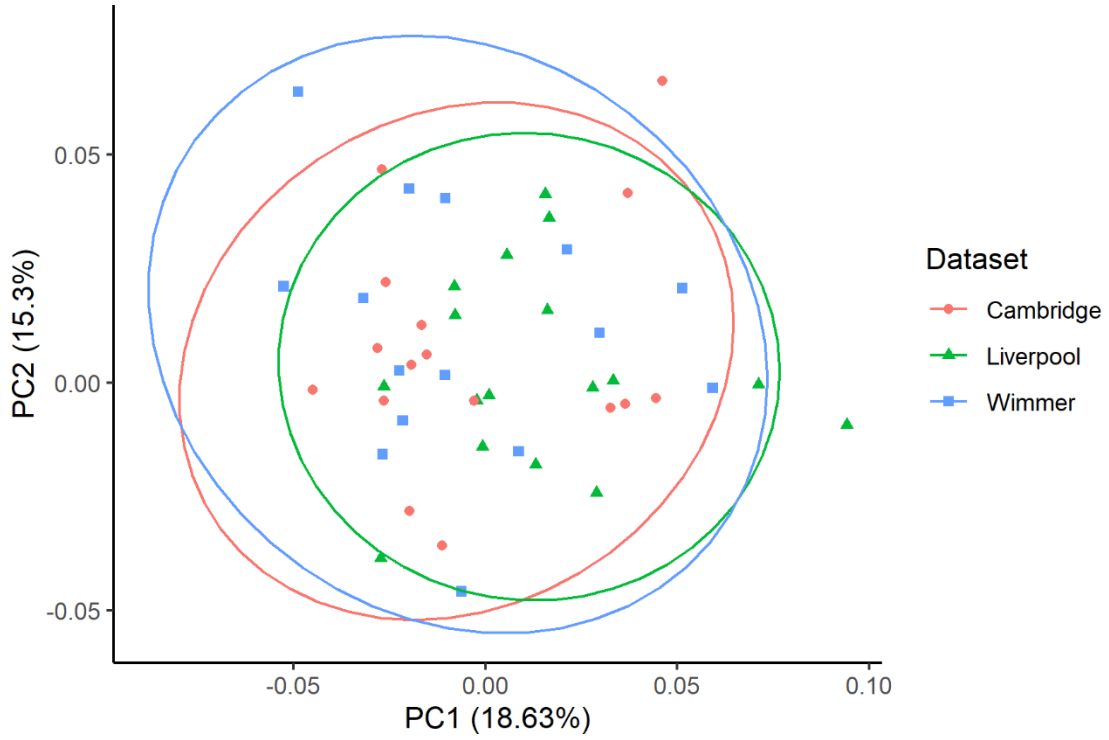

SF1: Adult morphospace distribution along PC1 and PC2 by dataset coded for dataset. Ellipses represent 95% CI.

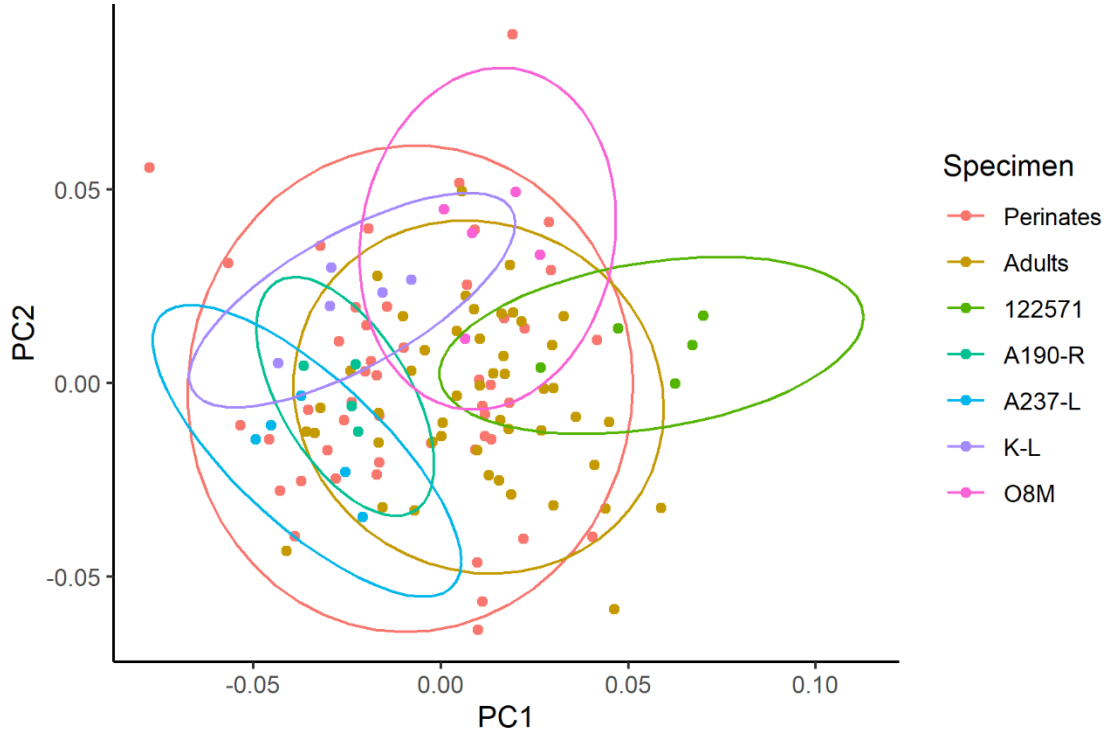

682

683 SF2: PC1 and PC2 of configuration shapes with repeated specimens. Ellipses represent 95% CI.

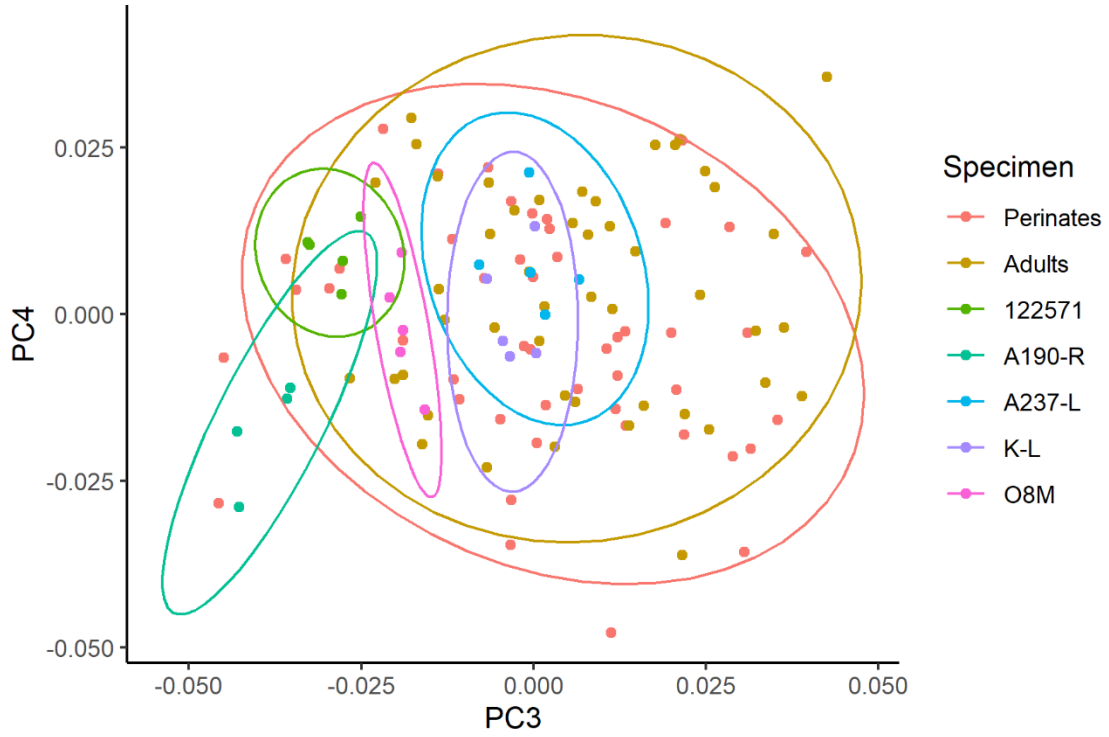

684

685 SF3: PC3 and PC4 of configuration shapes with repeated specimens. Ellipses represent 95% CI.

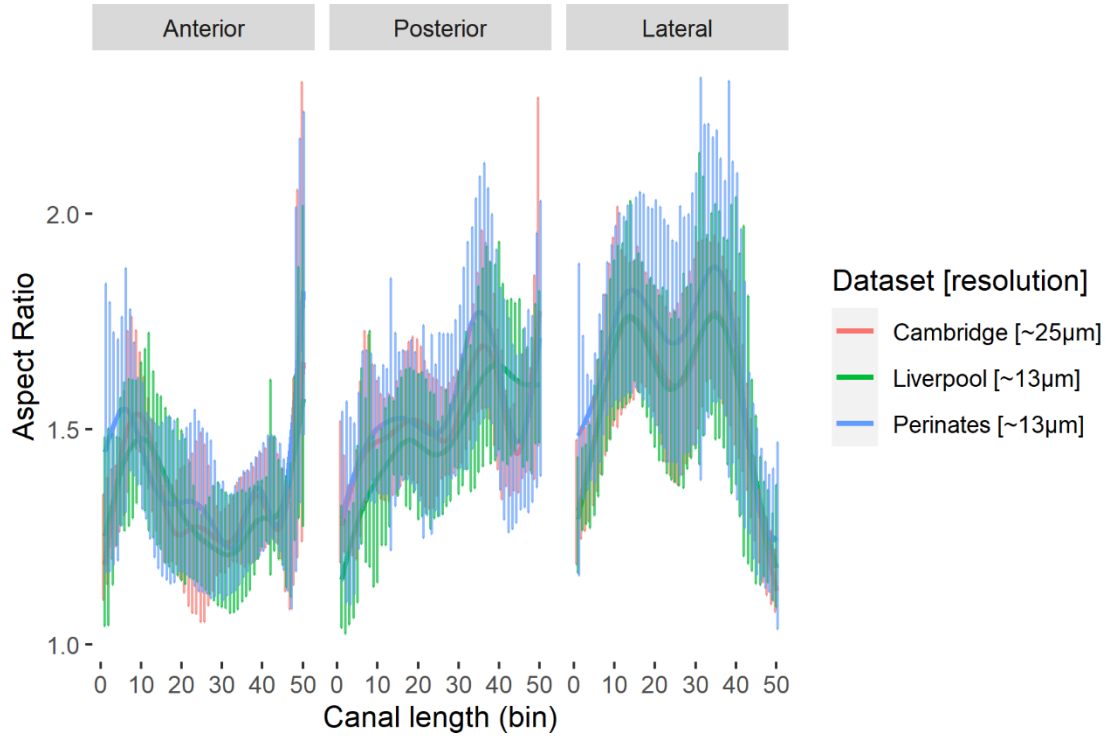

686

687 SF4: Aspect ratio. Results are grouped by dataset.

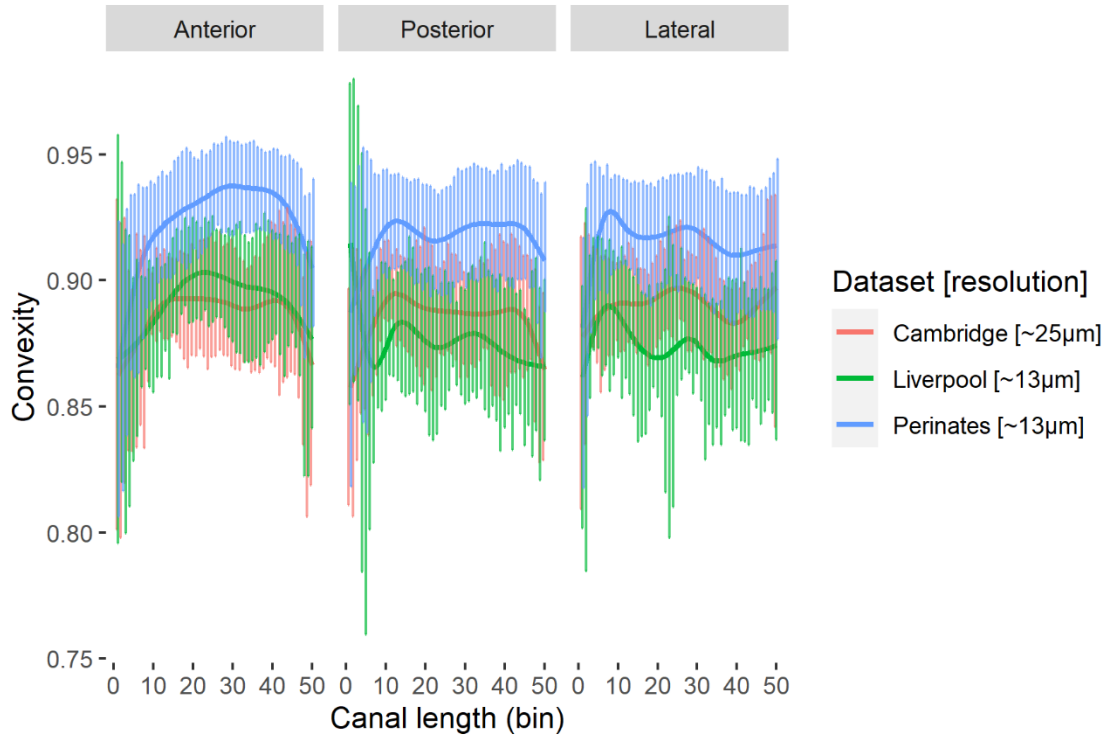

688

689 SF5: Convexity. Results are grouped by dataset.

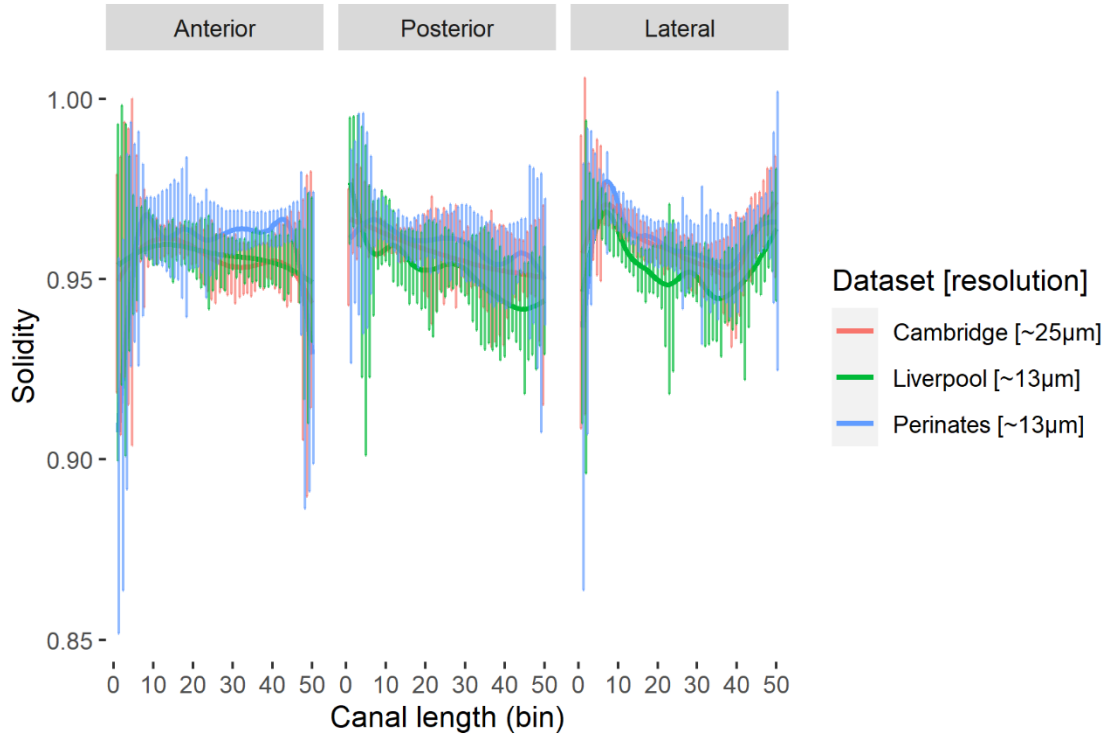

690

691 SF6: Solidity. Results are grouped by dataset.

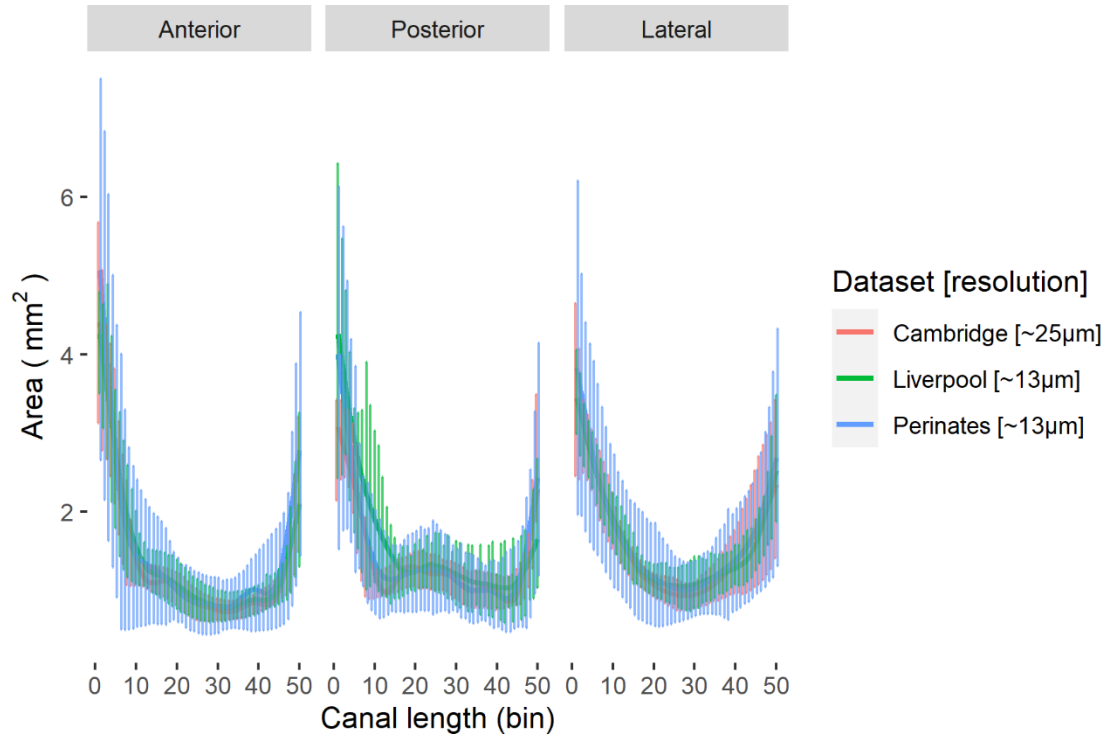

692

693 SF7: Cross-sectional area. Results are grouped by dataset.